Crystallinities and Light Emitting Properties of Nanostructured SiGe Alloy Prepared by Pulsed Laser Ablation in Inert Background Gases

PROCEEDINGS OF SPIE REPRINT

SPIE—The International Society for Optical Engineering

Reprinted from

Laser Applications in Microelectronic and Optoelectronic Manufacturing IV

25–27 January 1999
San Jose, California

Volume 3618

Crystallinities and Light Emitting Properties of Nanostructured SiGe Alloy Prepared by Pulsed Laser Ablation in Inert Background Gases

Takehito Yoshida, Yuka Yamada, Nobuyasu Suzuki, Toshiharu Makino,
Takaaki Orii*, Kouichi Murakami**,
David B. Geohegan***, Douglas H. Lowndes***, and Michael J. Aziz****

Matsushita Research Institute Tokyo, Inc., 3-10-1 Higashimita, Tama-ku, Kawasaki 214-8501, Japan
*Institute of Applied Physics, Univ. of Tsukuba, Tsukuba, Ibaraki 305-0006, Japan
** Institute of Materials Science, Univ. of Tsukuba, Tsukuba, Ibaraki 305-0006, Japan
***Solid State Division, Oak Ridge National Lab., Oak Ridge, TN 37831-6056
****Division of Applied Science, Harvard Univ., 29 Oxford Street Cambridge, MA 02138

ABSTRACT

For studying the material properties of nanostructured group IV materials, we have developed a pulsed laser ablation method into inert background gases. SiGe alloy nanocrystallites have possibility of novel band structure engineering by controlling not only compositions but also particle sizes. An ArF excimer laser was focused onto the surface of the powder-sintered Si_xGe_{1-x} target. During the laser ablation, He gas was introduced into a vacuum chamber and was maintained at a constant pressure. Size distribution of the Si_xGe_{1-x} ultrafine particles decreases with decreasing composition x under fixed conditions of deposition such as background gas pressure. Raman scattering spectra of the deposited SiGe ultrafine particles show three peaks ascribed to mixed crystalline SiGe after annealing, and the linewidths of these peaks broaden due to the reduced size of the crystallites. The frequencies and intensities of the peaks depend on the composition x. Visible PL spectra have broad peaks from 2.25 eV to 2.10 eV, at room temperature. The peak positions show blue shifts with increasing x. Electroluminescent diodes with the $Si_{0.8}Ge_{0.2}$ nanocrystallite active region were fabricated, and emit visible light peaked at around 1.8 eV, at room temperature.

Keywords: silicon-germanium alloy, nanocrystallites, pulsed laser ablation, Raman scattering, electroluminescence

1. INTRODUCTION

Ever since visible photoluminescence (PL) spectra were observed in nanometer-sized silicon (Si) [1-4], extensive studies have been carried out on nanometer-sized structures of group IV materials. In particular, the strong PL from porous Si has attracted much attention and much research has been undertaken to clarify its origin [5]. Furthermore, SiGe alloys have the capabilities of band structure engineering by controlling the composition [6], and there have been several reports on optical properties of porous SiGe [7,8]. When we discuss the optical properties of nanoscaled group IV materials as one of the quantum confinement effects, it is significant to adopt another approach using the nanoscale "spherical" structures which have well-controlled size and surface chemical structure. For this purpose, pulsed laser ablation (PLA)[9] into a background gas has been applied to the preparation of Si ultrafine particles [10-13]. Werwa et al.[10] reported that the minimum diameter of Si ultrafine particles was about 2 nm in laser ablation into a pulsed inert gas. Yoshida et al.[12] reported that the size distribution of Si nanocrystallites was controlled by varying the background gas pressure. Deohegan et al.[14] confirmed that the ejected species condensed into nanoparticles in the background gases. Furthermore, PLA has the potentialities for use in the deposition of complex materials with congruent transfer of the target composition [9,15], and SiGe thin films have been prepared using this method [16]. However, there have been few studies where alloy nanocrystallites are produced using PLA in background gases.

Recently, some research groups have focused on electroluminescence (EL) properties as well as on PL properties because the EL of the nanoscaled Si structures is suited to optoelectronic device applications. Most EL Si structures have been thinned to "porous" structures formed by liquid phase anodization.[5] EL of porous Si was first observed during anodic oxidation in an electrolyte solution.[17] Porous Si EL devices operating in the atmosphere have been studied with solid-state

* Present address: The Institute of Physical and Chemical Research (RIKEN), 2-1 Hirosawa, Wako-shi, Saitama 351-0198, Japan

Part of the SPIE Conference on Laser Applications in Microelectronic and Optoelectronic Manufacturing IV • San Jose, California • January 1999
SPIE Vol. 3618 • 0277-786X/99/$10.00

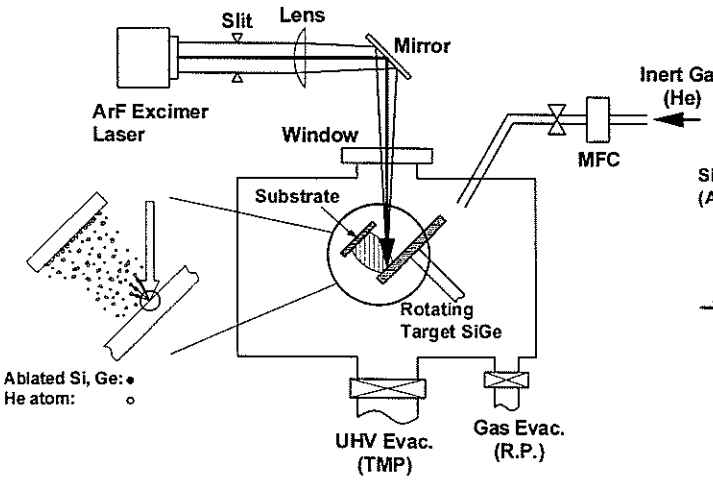

Fig.1. Schematic of the preparation system of SiGe alloy nanocrystallites using pulsed laser ablation in a reduced-pressure inert background gas.

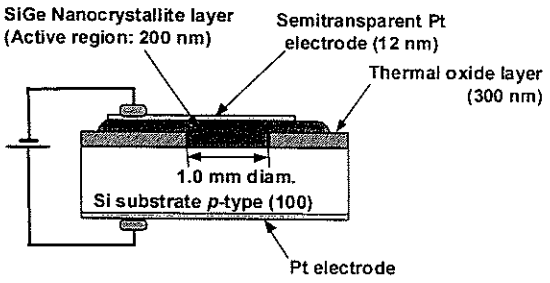

Fig. 2. Schematic cross-sectional view of the electro-luminescent (EL) diode. The structure is (semitrans-parent Pt electrode)/(SiGe nanocrystallite layer)/(*p*-type Si) /(Pt electrode).

contacts, including semitransparent metal-contacted Schottky junction diodes,[18-20] *p-n* homojunction diodes [21-24] and *p-n* heterojunction diodes.[25-28] Besides the porous Si, Qin et al. developed a visible EL device of the low operational voltage (> 4 V) in gold (Au)-contacted extra thin (4 nm) Si-rich Si oxide films deposited by magnetron sputtering.[29] Nassiopoulos et al. observed visible EL from Si nanopillars formed using highly anisotropic reactive etching and thinning thermal oxidation.[30]

In this work, we adopt the PLA in a constant pressure inert background gas. A sintered mixture of Si and Ge powders is used as a target. We characterize structures and optical properties of SiGe alloy nanocrystallites prepared by the PLA in inert background gas. In addition, we fabricate an EL diode with the $Si_{0.8}Ge_{0.2}$ alloy nanocrystallite active region, using the PLA in inert background gases as one of the physical vapor deposition (PVD) methods, aiming reasonable operational voltage (several - 25 V). We characterize electrical conductivity, dependence of EL intensity on excitation current and luminescence spectrum. Our fabrication method is compatible with the established Si large scale integrated (LSI) technology because the PVD-like process is suitable for successive film stacking and etching of fine patterns.

2. EXPERIMENTAL PROCEDURE

In order to deposit Si and Ge, which have different melting points and vapor pressures, at the same time by laser ablation, an appropriate target should be a mixture of Si and Ge with high purity. Thus, sintered SiGe targets were fabricated as follows. Si and Ge powders with the size of μm order and high purity of 6N were mixed without binder and sintered using a hot press system in an inert gas. Then, we could obtain Si_xGe_{1-x} (x = 0.18, 0.82) sintered targets of 2-inch diameter with purity over 4N. The alloy composition x of the sintered target was determined using inductively coupled plasma optical emission spectroscopy (ICPS).

SiGe ultrafine particles were prepared using PLA of the sintered SiGe target in an inert background gas at constant reduced pressure. A schematic diagram of the laser ablation apparatus used in this study is shown in **Fig. 1**. After the vacuum chamber was evacuated to 1.0×10^{-6} Pa, helium (He) gas was introduced into the chamber and was maintained at a constant pressure (333 Pa) using a differential evacuation system. An argon-fluoride (ArF) excimer laser (λ: 193 nm, energy density: 1.0 J/(cm^2·pulse), pulse duration: 12 ns, repetition rate: 10 Hz) beam was focused onto a 3×1 mm^2 rectangular spot at the surface of the sintered SiGe target of 2-inch diameter. Then, a plume of ejected species was created and extended almost perpendicular to the target surface. The target was rotated at 8 rpm. As described above, the size of the mixed powders of the sintered target was of μm order, which is much smaller than the spot size of the irradiated laser beam. Thus, the ejected species can have a mixed composition. A deposition substrate was located at a distance of 10 mm normal to the target. The species ejected from the target condensed during flight in a background gas [14] and then were deposited as ultrafine particles on the substrate [12]. The substrate was kept at room temperature during the deposition process. Finally, the deposited substrates were annealed in dry nitrogen (N_2) at 800℃ for 10 min., using an usual resistance-heating furnace.

Fig. 3. SEM photographs of as-deposited Si_xGe_{1-x} ultrafine particles. The average size of the ultrafine particles decreases with decreasing composition x.

A schematic cross-sectional view of the EL diode is shown in **Fig. 2**. To fabricate the EL diode, (100) oriented *p*-type Si wafers with a resistivity of 0.02 Ω•cm were used as substrates. Thermal oxide layers were formed with a thickness of 300 nm for the isolation dielectrics. Electrically active regions with a diameter of 1.0 mm were defined by removing the thermal oxide with $HF+NH_4F$ solution. The Si nanocrystallite layers were deposited by the above PLA method. Thermal annealing was carried out at 825 °C for 10 min in N_2 , using a rapid thermal annealing system. In order to form a contact with the Si nanocrystallite layers, semitransparent platinum (Pt) films were deposited with a thickness of 12 nm. The EL active regions were Si nanocrystallite layers with an area of 7.9×10^{-3} cm^2 (1.0 mm diameter circle) and a thickness of about 200 nm.

Scanning electron microscope (SEM) observation was employed to evaluate the particle size of the deposits. The average composition of the deposited particles was evaluated using ICPS measurement. Raman scattering spectra were measured with a filtered single monochromator (Jasco TRS-600) system in a backscattering geometry. Excitation was provided by the 514.5 nm Ar^+ ion laser line. A CCD system (Photometrics TK512CB) was used as a detector. To prevent damage of samples by the laser and/or a change of the Raman spectrum during measurements, the laser power was chosen to be less than 4 mW. In the Raman scattering measurement, fused quartz was used for the deposition substrate. Furthermore, PL

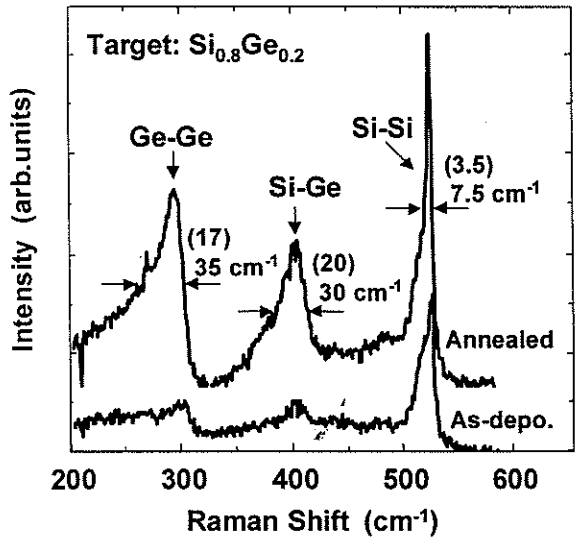

Fig. 4. Raman spectra of $Si_{0.8}Ge_{0.2}$ alloy nanocrystallites. Three Raman peaks intrinsic to crystalline SiGe alloys are observed.

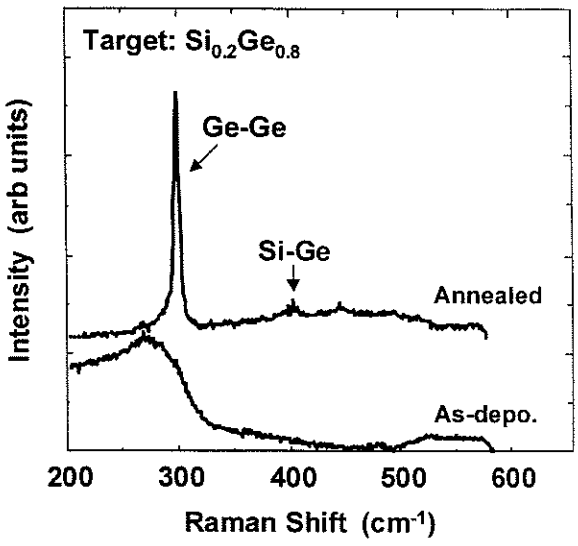

Fig. 5. Raman spectra of $Si_{0.2}Ge_{0.8}$ alloy nanocrystallites. Ge-Ge and Si-Ge peaks are observed after annealing.

measurements were performed at room temperature using a single polychromator (Jasco CT-25C) system with a cooled MOS linear-image sensor unit (Hamamatsu C4834-02) as a detector. An Ar^+ ion laser (λ: 488.0 nm, power: 5 mW) was used as an excitation light source. The spectral sensitivity of the measurement system was calibrated using a halogen standard lamp.

We measured the current-voltage (*I-V*) characteristics of the EL diodes. The dependence of the integrated EL intensity on the diode current was investigated at room temperature. The EL intensity was measured by a photomultiplier (Hamamatsu Photonics R3896). The EL spectra were measured at room temperature using a single polychromator system (Acton SpectraPro-275) with a cooled FET-CCD image sensor unit (Hamamatsu M6296-01) as a detector.

3. EXPERIMENTAL RESULTS

The as-deposited Si_xGe_{1-x} ultrafine particles were observed using SEM to clarify the dependence of the particle size on the composition x. These results are shown in **Fig. 3**. Nanometer-sized ultrafine particles are observed. Furthermore, the average size decreases with decreasing x under the fixed processing conditions. The average composition of the ultrafine particles deposited on the Al_2O_3 substrate using the $Si_{0.82}Ge_{0.18}$ target was evaluated by ICPS. The total ratio (at.%) of Si:Ge of the deposited ultrafine particles was obtained as 78.9:21.1. From this result, it is revealed that our PLA process can transfer as a whole the composition of the target to the deposits.

Figure 4 shows Raman scattering spectra of the $Si_{0.8}Ge_{0.2}$ ultrafine particles before and after the annealing. Three Raman peaks ascribed to the vibrations of Ge-Ge, Si-Ge and Si-Si pairs are observed at 292, 400 and 520 cm^{-1}, respectively. These peaks are intrinsic to the crystalline SiGe alloy system.[31] The intensities of theses peaks increase after annealing. This result shows that crystallization progressed after the annealing process. **Figure 5** shows Raman scattering spectra of the $Si_{0.2}Ge_{0.8}$ ultrafine particles before and after the annealing. A broad peak appears at 200-300 cm^{-1} before the annealing, which is associated with amorphous Ge.[4] After annealing, Ge-Ge and Si-Ge peaks are observed at 298 and 400 cm^{-1}, respectively.[31] The Si-Si peak cannot be observed. As a result, the Ge-rich ultrafine particles, which are amorphous-like before annealing, are crystallized after the annealing process.

Figures 6 (a), (b), and (c) show the PL spectrum from the SiGe nanocrystallites of which compositions are $Si_{0.8}Ge_{0.2}$, $Si_{0.2}Ge_{0.8}$, and pure Ge, respectively. In all of them, broad green PL bands appear at room temperature. The PL intensities increase after the annealing. These PL spectra have broad peaks from 2.25 eV to 2.10 eV, with a low energy shoulder around 1.8 eV. The peak positions showed blue shifts with increasing silicon content x. There is a tendency where the shoulder intensity increases with increasing silicon content x.

Figure 7 shows the *I-V* characteristics of a typical EL diode in linear scale. In the pure Si nanocrystallite, a weak rectifying behavior is observed. In the $Si_{0.8}Ge_{0.2}$ nanocrystallite, the reverse-biased curve seems a soft-breakdown characteristics. The series resistances *Rs* in the forward bias regions were estimated to be 70 Ω and 170 Ω, in $Si_{0.8}Ge_{0.2}$ and pure Si,

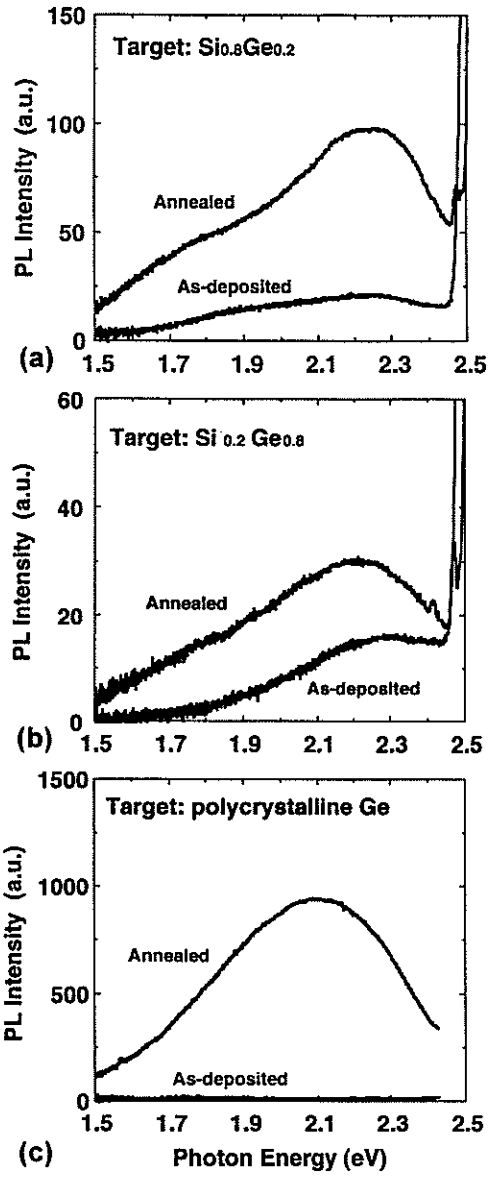

Fig.6. PL spectra from SiGe alloys and pure Ge nanocrystallites. (a) $Si_{0.8}Ge_{0.2}$, (b) $Si_{0.2}Ge_{0.8}$, (c) Pure Ge.

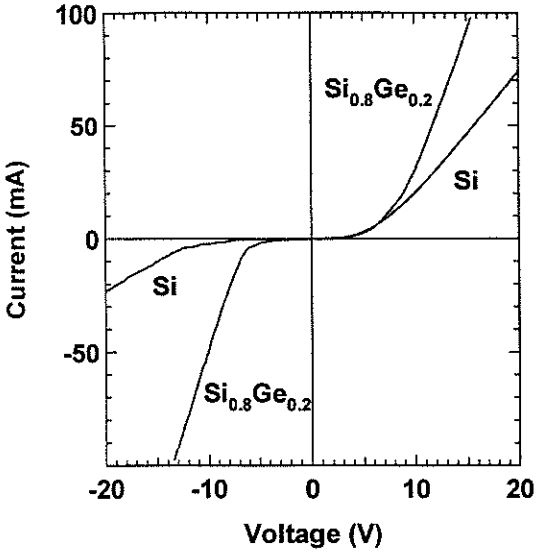

Fig.7. *I-V* characteristics of the EL diodes with the $Si_{0.8}Ge_{0.2}$ alloy and pure Si nanocrystallite layers as the active regions.

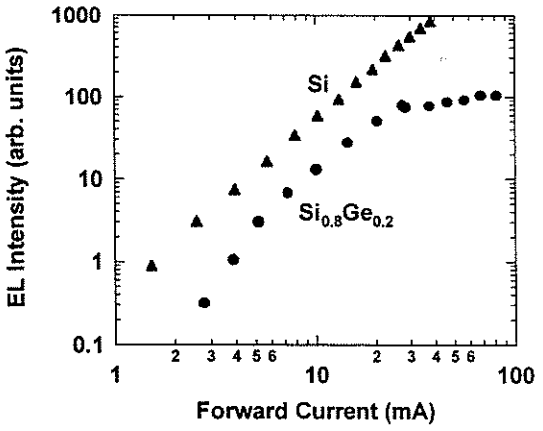

Fig.8. Integrated EL intensity I_{EL} as afunction of the forward current j, for the EL diodes with the $Si_{0.8}Ge_{0.2}$ alloy and pure Si nanocrystallite active layers.

respectively. The onsets of the light emission, measured with the photomultiplier, were forward-biased dissipation power about 10 mW, in both the pure Si and the $Si_{0.8}Ge_{0.2}$ nanocrystallite EL diodes. **Figure 8** shows the integrated EL intensity I_{EL} as a function of the forward current j in a log-log scale. In the pure Si, it is evident that the dependence of I_{EL} on j is according to a rapid power law.[32] Namely, I_{EL} is proportional to j^m, m=2.2. In the $Si_{0.8}Ge_{0.2}$, the rapid power law was also observed as a relation between I_{EL} and j. However, I_{EL} saturated in the forward current range more than 3 mA. **Figure 9** shows the measured EL spectra of both the pure Si and the $Si_{0.8}Ge_{0.2}$ nanocrystallite EL diodes. Dissipation powers of the pure Si and the $Si_{0.8}Ge_{0.2}$ were 0.86 W (20 V, 43 mA) and 0.82 W (12 V, 68 mA), respectively. Both spectra have peaks around 1.8 eV and shoulders around 2.2 eV. The peak and shoulder positions of the $Si_{0.8}Ge_{0.2}$ looks slightly blue-shifted, in comparison with those of the pure Si.

4. DISCUSSION

There have been several reports on the study of the dependence of the Raman scattering spectra on the composition x of bulk Si_xGe_{1-x} alloys.[31,33] The frequencies and linewidths (FWHM) of three Raman peaks ascribed to vibrations of Ge-Ge, Si-Ge, and Si-Si pairs strongly depend on the composition x. The frequencies of these peaks in **Figs. 4** and **5** correspond well to those of the bulk $Si_{0.8}Ge_{0.2}$ and $Si_{0.2}Ge_{0.8}$ alloys reported in Ref. 31. This result shows that the composition is maintained in the SiGe alloy nanocrystallites deposited by PLA in an inert background gas.

However, the FWHM of the three Raman peaks in our experiment are about 2 times broader than that of the bulk alloys in Ref. 31. The FWHM values of this work are indicated in **Fig. 4**. Also the FWHM values in Ref. 31 are indicated in the brackets. According to a spatial correlation model, finite size effects relax the q-vector selection rule and this relaxation of the momentum conservation leads to a broadening and downshift of the Raman spectrum.[34] To

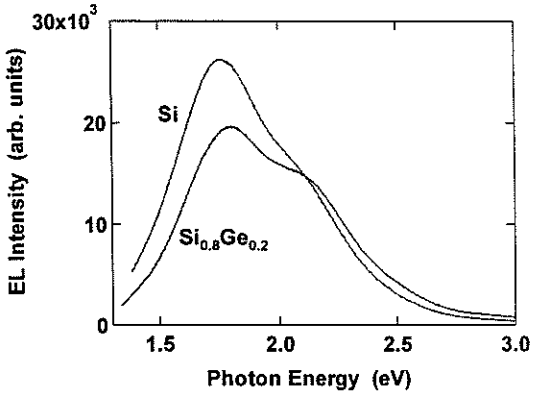

Fig.9. EL spectra at room temperature, for the EL diodes with the $Si_{0.8}Ge_{0.2}$ alloy and pure Si nanocrystallite active layers.

clarify the finite size effects shown in the Raman spectrum, Raman scattering measurements were also performed for Si nanocrystallites. **Figure 10** shows Raman scattering spectra of the Si nanocrystallites before and after oxidation annealing.[35] The dash-dotted line indicates the peak position of the bulk single-crystalline Si. The Raman peak of the bulk Si was symmetric and had a FWHM of 3.7 cm^{-1} in this measurement. It was found that the Si nanocrystallites have a broader and lower frequency peak in comparison with the bulk Si. The average diameter of the as-deposited Si nanocrystallites in **Fig. 10** was estimated to be about 11 nm using the strong phonon confinement model.[36] This result is in good agreement with the result obtained from high-resolution transmission electron microscopy (TEM).[12,35] Furthermore, the annealing process causes a much broader shape and lower frequency, as shown in **Fig. 10**. This result proposes that the oxidation annealing caused a size reduction of the core of the Si nanocrystallite.

The broadened FWHMs of the Raman peaks in SiGe alloy nanocrystallites must also be caused by the reduction of the particle size. **Figure 11** shows the Si-Si peak of the $Si_{0.8}Ge_{0.2}$ alloy nanocrystallites after the annealing in **Fig. 4**. The FWHM broadens to 7.0 cm^{-1}, especially to lower frequencies compared to the Si nanocrystallites. This result cannot be explained by only the reduced size of the SiGe nanocrystallites. The inclusion of Ge as impurities in Si should increase lattice disorder which would result in the relaxation of the q-vector selection rule. Furthermore, Okada and Iijima indicated the existence of the strong stress in oxidized Si particles from the study of the oxidation properties.[37] Such a stress especially in the nanocrystallites can exist in the SiGe nanocrystallites and cause the strain effects, which also results in the broadening of the Raman peaks.

Consequently, Raman scattering spectra of Si_xGe_{1-x} alloy nanocrystallites depend on the composition x. The peak shifts of nanocrystalline and bulk SiGe alloys can be explained by the same mechanism. Furthermore, the linewidths broaden to lower frequencies compared to the bulk alloys. This property is considered to be derived from the synergistic effect of the finite size confinement and the lattice disorder.

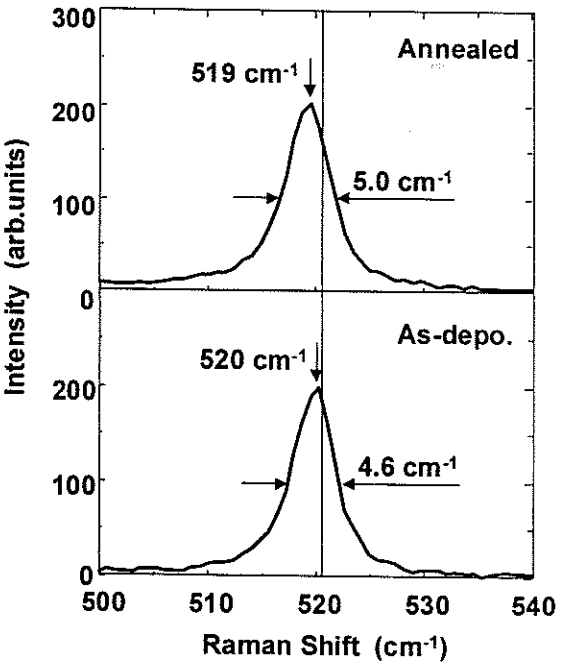

Fig.10. Raman spectra of Si pure nanocrystallites. Dash-dotted line indicates the peak position of the bulk single-crystalline Si. FWHM of the bulk Si was 3.7 cm^{-1} in this measurement.

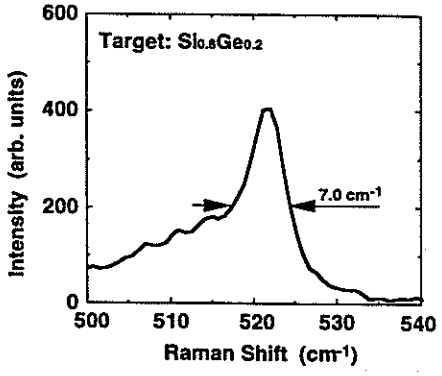

Fig.11. Raman peak ascribed to Si-Si vibration of the $Si_{0.8}Ge_{0.2}$ alloy nanocrystallites after annealing in Fig. 4. FWHM broadens to 7.0 cm^{-1}.

In **Figs. 6**, the PL spectra have broad peaks from 2.25 eV to 2.10 eV, with a low energy shoulder around 1.8 eV. The peak positions showed blue shifts with increasing composition (silicon content) x. This tendency is consistent with bandgap dependence on the composition x, in the bulk SiGe alloy.[6] On the other hand, in the both EL spectra, there are peaks around 1.8 eV and shoulders around 2.2 eV, in Fig. 9. The peak and shoulder positions of the $Si_{0.8}Ge_{0.2}$ looks slightly blue-shifted, in comparison with those of the pure Si. It can be said that the green band emission (peaked around 2.2 eV) and the red band emission (peaked around 1.8 eV) are associated with "shallow" and "deep" localized states, respectively. Furthermore, in general, the capture cross section of the non-radiative center P_{NR} is described by the following formura:[38]

$$P_{NR}=W_0(h\omega_0/kT)\exp(-(2R/Re)-(E_A/kT^*)) \qquad (1)$$

$$T^*=(h\omega_0/2k)\coth(h\omega_0/2kT), \qquad (2)$$

where ω_0, E_A, R, and Re stand for the phonon frequency, activation energy of a localized state, distance between an electron and a non-radiative center, and extent of electron wave funcion, respectively. According to equ. (1), the shallower activation energies of the localized states are, the higher probabilities of the non-radiative recombinations are, with increasing temperature. In our experimental conditions, dissipation power densities in the typical EL measurements were about 40 times higher than that of the PL measurements, because the dissipation power densities of the EL measurements and the PL measurements were about 100 W/cm^2 and 2.5 W/cm^2. Since the measuring temperatures of the EL should be much higher that that of the PL, quenching of the light emitting associated with the shallow levels became remarkable in the EL measurements. We suggest that this is the reason why the EL spectra had 1.8 eV peak and 2.2 eV shoulder in **Fig. 9**, though the PL spectra in **Figs. 6** had 2.25-2.10 eV peaks and 1.8 eV shoulders. However, we have not had enough data to discuss dependence of the emission peak position on the composition x.

In **Fig. 7**, the *I-V* characteristics of the EL diodes had only weak rectifying behavior. In our previous study, we observed the strong rectifying behaviors, where an usual resistance-heating furnace was used for the nanocrystallites active layer annealing.[32] Reactor of the rapid thermal processing system in this work can be evacuated to 1×10^{-3} Pa by a TMP, before introducing pure N_2 ambient gas. On the other hand, the usual resistance-heating furnace was atmospheric pressure operation without evacuation system. Therefore, we propose that the rectifying behaviors were related to residual oxygen or other contaminant gases in the annealing ambient.

According to **Fig. 8**, in both the pure Si and the $Si_{0.8}Ge_{0.2}$ nanocrystallite EL diodes, the integrated EL intensity I_{EL} had rapid nonlinear dependence on the forward current density j. As we mentioned in previous study,[32] it seems that the excitation mechanism for the EL is associated with impact ionization induced by hot carrier injection and successive radiative recombination. However, the I_{EL} saturation phenomenon in the $Si_{0.8}Ge_{0.2}$ nanocrystallite EL diode has not been understood yet. Further study is in progress.

5. CONCLUSION

SiGe alloy nanocrystallites have been obtained using excimer laser ablation of sintered SiGe targets in a constant-pressure inert background gas. The deposited Si_xGe_x nanocrystallites have the same alloy composition x as the target. The Raman peaks intrinsic to crystalline alloys have broadened to lower frequencies compared with those of bulk alloys. This should be explained in terms of the synergistic effect of the finite size confinement and the lattice disorder. Furthermore, we observed visible PL spectra which had broad peaks from 2.25 eV to 2.10 eV, at room temperature. The peak positions showed blue shifts with increasing x. Electroluminescent diodes with the $Si_{0.8}Ge_{0.2}$ nanocrystallite active region have successfully been fabricated, and have emitted visible light peaked at around 1.8 eV, at room temperature.

6. ACKNOWLEDGEMENTS

The authors would like to express their thanks to Professor. S. Onari and Associate Professor. K. Matsuishi (Univ. of Tsukuba) and Professor. T. Arai (Ishinomaki Sensyu Univ.) for their fruitful discussion of the optical properties and spectroscopy of mesoscopic materials.

This study was partially supported by a Grant in Aid for International Scientific Research Program: Joint Research of the Ministry of Education, Science and Culture.

7. REFERENCES

1. S. Furukawa and T. Miyasato, Jpn. J. Appl. Phys. 27, L2207 (1988).
2. H. Takagi, H. Ogawa, Y. Yamazaki, A. Ishizaki, and T. Nakagiri, Appl. Phys. Lett. 56, 2379 (1990).
3. L. T. Canham, Appl. Phys. Lett. 57, 1046 (1990).
4. Y. Maeda, N. Tsukamoto, Y. Yazawa, Y. Kanemitsu, and Y. Masumoto, Appl. Phys. Lett. 59, 3168 (1991).
5. D. J. Lockwood, *Light Emission in Silicon from Physics to Devices*, Academic Press, San Diego, 1998.
6. R. Braunstein, A. R. Moore, and F. Herman, Phys. Rev. 109, 695 (1958).
7. S. Gardelis, J. S. Rimmer, P. Dawson, B. Hamilton, R. A. Kubiak, T. E. Whall, and E. H. C. Parker, Appl. Phys. Lett. 59, 2118 (1991).

8. A. Ksendzov, R. W. Fathauer, T. George, W. T. Pike, R. P. Vasquez, and A. P. Taylor, Appl. Phys. Lett. 63, 200 (1993).
9. D. H. Lowndes, D. B. Deohegan, A. A. Puretzky, D. P. Norton, and C. M. Rouleau, Science 273, 898 (1996).
10. E. Werwa, A. A. Seraphin, L. A. Chiu, Chuxin Zhou, and K. D. Kolenbrander, Appl. Phys. Lett. 64, 1821 (1994).
11. T. Makimura, Y. Kunii, and K. Murakami, Jpn. J. Appl. Phys. 35, 4780 (1996).
12. T. Yoshida, S. Takeyama, Y. Yamada, and K. Mutoh, Appl. Phys. Lett. 68, 1772 (1996).
13. Y. Yamada, T. Orii, I. Umezu, S. Takeyama, and T. Yoshida, Jpn. J. Appl. Phys. 35, 1361 (1996).
14. D. B. Geohegan, A. A. Puretzky, G. Duscher, and S. Pennycook, Appl. Phys. Lett. 72, 2987 (1998).
15. D. B. Chrisey and G. K. Hubler, *Pulsed Laser Deposition of Thin Films*, Wiley, New York, 1994.
16. F. Antoni, E. Fogarassy, C. Fuchs, J. J. Grob, B. Prevot, and J. P. Stoquert, Appl. Phys. Lett. 67, 2072 (1995).
17. A. Halimaoui, C. Oules, G. Bomchil, A. Bsiesy, F. Gaspard, R. Herino, M. Ligeon, and F. Muller, Appl. Phys. Lett. 59, 304 (1991).
18. A. Richter, P. Steiner, F. Kozlowski, and W. Lang, IEEE Electron Device Lett. EDL-12, 691 (1991).
19. N. Koshida and H. Koyama, Appl. Phys. Lett. 60, 347 (1992).
20. P. Steiner, F. Kozlowski, and W. Lang, IEEE Electron Device Lett. EDL-14, 317 (1993).
21. Z. Chen, G. Bosman, and R. Ochoa, Appl. Phys. Lett. 62, 708 (1993).
22. P. Steiner, F. Kozlowski, and W. Lang, Appl. Phys. Lett. 62, 2700 (1993).
23. J. Linnros and N. Lalic, Appl. Phys. Lett. 66, 3048 (1995).
24. N. Lalic and J. Linnors, J. Appl. Phys. 80, 5971 (1996).
25. T. Futagi, T. Matsumoto, M. Katsuno, Y. Ohta, H. Mimura, and K. Kitamura, Jpn. J. Appl. Phys. 31, L616 (1992).
26. P. C. Sercel, D. Kwon, T. Vilbrandt, W. D. Yang, J. Hautala, J. D. Cohen, and Hao Lee, Appl. Phys. Lett. 68, 684 (1996).
27. F. Namavar, H. P. Maruska, and N. M. Kalkhoran, Appl. Phys. Lett. 60, 2514 (1992).
28. H. P. Maruska, F. Namavar, and N. M. Kalkhoran, Appl. Phys. Lett. 61, 1338 (1992).
29. G. G. Qin, A. P. Li, B. R. Zhang, and B-C Li, J. Appl. Phys. 78, 2006 (1995).
30. A. G. Nassiopoulos, S. Grigoropoulos, and D. Papadimitriou, Appl. Phys. Lett. 69, 2267 (1996).
31. M. Balkanski, *Light Scattering in Solids*, p. 326, Flammarion, Paris, 1971.
32. T. Yoshida, Y. Yamada, T. Orii, J. Appl. Phys. 83, 5427 (1998).
33. W. J. Brya, Solid State Commun. 12, 253 (1973).
34. H. Richter, Z. P. Wang, and L. Ley, Solid State Commun. 39, 625 (1981).
35. T. Yoshida, Y. Yamada, S. Takeyama, T. Orii, I. Umezu, and Y. Makita, Proc. SPIE 2888, 6 (1996).
36. I. H. Campbell and P. M. Fauchet, Solid State Commun. 58, 739 (1986).
37. R. Okada and S. Iijima, Appl. Phys. Lett. 58, 1662 (1991).
38. R. Englman and J. Jortner, Molecular Phys. 18, 145 (1970).